Applications of resolvent analysis in fluid mechanics

Beverley McKeon
California Institute of Technology
mckeon@caltech.edu

July 22, 2019

1 Introduction

1.1 Objectives and prerequisites

These notes are intended to provide a description of some aspects of applications of resolvent analysis in fluid mechanics. They are targeted at students beginning research in this or related area, with the goal of providing a bridge between the generic linear algebra of textbooks and the archival journal articles implementing these techniques.

With regards to mathematical techniques, a working understanding of fundamental concepts of linear algebra, and in particular the singular value decomposition, as well a familiarity with the goals underlying modal analysis are assumed. Requiring more background in fluid mechanics, the reader will already be familiar with the formulation of resolvent analysis from the Navier-Stokes equations. These notes outline approaches to gaining insight into the characteristics of fluid system by viewing the governing equations in terms of linear dynamics driven by endogenous (nonlinear) or exogenous forcing. Such systems may exhibit laminar or turbulent behavior, may be forced or unforced, and may perhaps be under the influence of control actuation.

Physical interpretation of resolvent modes, the importance of mode weights and techniques for data reconstruction, and the incorporation of control into the analysis are covered.

1.2 Terminology and resolvent formulation

In these notes, we use the terminology outlined in "Elements of resolvent methods in fluid mechanics: notes for an introductory short course" by A. S. Sharma [1]. The concepts most important for this development are outlined below.

We first express the Navier-Stokes equations (NSE) in terms of state variable $\mathbf{q}(\mathbf{x}, t)$, with $\mathbf{x} = (x, y, z)$ corresponding to the spatial coordinates and t denoting time, in the form

$$\frac{\partial \mathbf{q}}{\partial t} = \mathcal{L}\mathbf{q} + \mathcal{N}(\mathbf{q}) + \mathbf{B}\zeta. \tag{1}$$

Terms that are linear with respect to $\mathbf{q}$ have been grouped as $\mathcal{L}\mathbf{q}$ and the (quadratic) nonlinear term is denoted by $\mathcal{N}$. An external forcing, $\mathcal{B}\zeta$, has been included to permit treatment of exogenous and/or control inputs; this can be set to zero in the absence of both.

The system can also be written in a more general "input-output" form by adding the following equation to the system description of Equation 1

$$\rho = \mathcal{C}\mathbf{q}. \tag{2}$$

Here the matrices $\mathcal{B}$ and $\mathcal{C}$ select the input and output of interest for the analysis which follows, with ρ being the output. For the purposes of this tutorial, we focus on the formulation of Equation 1.

For laminar flows, there exists a base flow which constitutes a solution of the NSE, and which can be determined *a priori*. In resolvent analysis of laminar flows, we are typically interested in the *exogenous* disturbances that can lead to large energy amplification, e.g. [2]. Thus nonlinear term $\mathcal{N}$ can be neglected and ζ can be used to represent the "noise" forcing that is most amplified, i.e. most dangerous, and therefore may play an important role in transition to turbulence.

For turbulent flows, equilibrium solutions of similar kind do not exist because the (gradients of the) Reynolds stresses arising from the nonlinear interactions of the fluctuations contained in $\mathcal{N}$ are required to sustain the flow. Thus $\mathcal{N}$ must be retained or modeled for a complete analysis.

The turbulent mean flow is given by the mean of $\tilde{\mathbf{q}}$ under the averaging procedure most appropriate to the flow under consideration, and fluctuations are defined in terms of the difference between the instantaneous and mean fields. Resolvent analysis assumes either that the mean flow is known, since

it will appear in the resolvent operator, or (much harder) that consistency of the results of a more in-depth analysis with the mean flow can be used as a constraint. We begin by assuming the mean flow.

For example, for a statistically stationary flow that is homogeneous in all but one spatial direction (say y), the mean flow is one-dimensional and determined from spatio-temporal integration over x, y and t, such that $\overline{\mathbf{q}}(y)$. Then the fluctuations are given by,

$$\tilde{\mathbf{q}}(\mathbf{x}, t) = \mathbf{q}(\mathbf{x}, t) - \overline{\mathbf{q}}(y). \tag{3}$$

Treatment of two, and even three-, dimensional and multi-component mean flows is possible using resolvent analysis, with the appropriate adjustment of Equation 3.

Let us specialize to consider the velocity field, $\mathbf{q} = \mathbf{u}$, and let $\mathcal{N}(\mathbf{q}) = \mathbf{f}$. After Fourier transforming the NSE in time and rearranging, the general formulation for resolvent analysis is

$$\hat{\mathbf{u}}(\mathbf{x}, \omega) = H(\omega)\hat{\mathbf{f}}(\mathbf{x}, \omega), \tag{4}$$

where

$$\hat{\mathbf{u}}(\mathbf{x}, \omega) = \int_{-\infty}^{\infty} e^{-i\omega t}\mathbf{u}(\mathbf{x}, t)dt, \tag{5}$$

and similarly for $\hat{\mathbf{f}}(\mathbf{x}, \omega)$.

$H(\omega)$ is the resolvent; its exact entries depend on the formulation of the NSE that has been utilized in deriving it. The inclusion or not of an eddy viscosity to account for scale interactions has been an ongoing topic of discussion, see, e.g. [3]; it is not included in the approach followed here. $H(\omega)$ constitutes a transfer function between an input (here, the forcing arising from nonlinear interactions of other frequencies) and the corresponding velocity response.

The resolvent may be analyzed using the Schmidt decomposition, which gives, at each ω,

$$H(\omega)\hat{\mathbf{f}}(\mathbf{x}, \omega) = \sum_{j \epsilon \mathbb{N}} \sigma_j(\omega)\langle\hat{\mathbf{f}}(\mathbf{x}, \omega), \phi_j(\mathbf{x}, \omega)\rangle\psi_j(\mathbf{x}, \omega). \tag{6}$$

The singular vectors, $\phi_j(\mathbf{x}, \omega)$ and $\psi_j(\mathbf{x}, \omega)$, constitute orthonormal bases and are known as the forcing and response modes, respectively. The singular values, or gains, $\sigma_j(\omega)$, order the basis functions. Here angle brackets denote

an inner product, interpretable here as the projection of the full $\hat{\mathbf{f}}(\mathbf{x},\omega)$ onto the forcing mode $\phi_j(\mathbf{x},\omega)$.

Denoting this by $\chi_j(\omega)$, we introduce mode weights, determined by the nonlinearity in a turbulent flow,

$$\chi_j(\omega) = \langle \hat{\mathbf{f}}(\mathbf{x},\omega), \phi_j(\mathbf{x},\omega) \rangle. \tag{7}$$

Then $\hat{\mathbf{u}}(\mathbf{x},\omega)$ and $\hat{\mathbf{f}}(\mathbf{x},\omega)$ may be expanded in terms of the forcing and response modes, obtained from the NSE with knowledge only of the mean velocity field, as follows,

$$\hat{\mathbf{u}}(\mathbf{x},\omega) = \sum_{j \epsilon \mathbb{N}} \chi_j(\omega)\sigma_j(\omega)\psi_j(\mathbf{x},\omega) \tag{8}$$

$$\hat{\mathbf{f}}(\mathbf{x},\omega) = \sum_{j \epsilon \mathbb{N}} \chi_j(\omega)\phi_j(\mathbf{x},\omega). \tag{9}$$

1.3 Example form of the resolvent

To give a concrete example of one form of the resolvent of the NSE, consider an incompressible flow in a Cartesian geometry with a one-dimensional, one-component mean flow, $\overline{U}(y)$. The Fourier transform of the NSE may now be performed in the homogeneous spatial directions, x and z, such that ω and t in Equation 5 may be replaced by $\mathbf{k} = (k_x, k_z, \omega)$ and (x, z, t), respectively. Then the resolvent formulation is simply

$$\begin{bmatrix} \hat{\mathbf{u}}(y,\mathbf{k}) \\ \hat{p}(y,\mathbf{k}) \end{bmatrix} = \left(-i\omega \begin{bmatrix} \mathbf{I} & \\ & 0 \end{bmatrix} - \begin{bmatrix} \mathcal{L}_{\mathbf{k}} & -\nabla \\ \nabla^T & 0 \end{bmatrix} \right)^{-1} \begin{bmatrix} \mathbf{I} \\ 0 \end{bmatrix} \hat{\mathbf{f}}(y,\mathbf{k}), \tag{10}$$

where $\mathcal{L}_{\mathbf{k}}$ is the (spatial) linear Navier-Stokes operator given by

$$\mathcal{L}_{\mathbf{k}} = \begin{bmatrix} -ik_x\overline{U} + \nabla^2/Re & -\partial_y\overline{U} & 0 \\ 0 & -ik_x\overline{U} + \nabla^2/Re & 0 \\ 0 & 0 & -ik_x\overline{U} + \nabla^2/Re \end{bmatrix}, \tag{11}$$

Here the gradient operator $\nabla = [ik_x, \partial_y, ik_z]$, the Laplacian $\nabla^2 = \partial_{yy} - \kappa^2$, ∂_y and ∂_{yy} denote the first and second derivatives with respect to y and the non-dimensionalization used determines the Reynolds number, Re. Focusing on the velocity fluctuations and defining $\mathbf{k}' \neq \mathbf{k}$, we can write

$$\hat{\mathbf{u}}(y,\mathbf{k}) = \mathcal{H}_{\mathbf{k}}\hat{\mathbf{f}}(y,\mathbf{k}) = \mathcal{H}_{\mathbf{k}}\mathbf{N}_{\mathbf{k}}(\hat{\mathbf{u}}(y,\mathbf{k}')). \tag{12}$$

The transfer function,

$$\mathcal{H}_{\mathbf{k}} = \begin{bmatrix} -i(\omega - k_x\overline{U}) - \nabla^2/Re_\tau & -\partial_y\overline{U} & 0 \\ 0 & -i(\omega - k_x\overline{U}) - \nabla^2/Re_\tau & 0 \\ 0 & 0 & -i(\omega - k_x\overline{U}) - \nabla^2/Re_\tau \end{bmatrix}^{-1}, \tag{13}$$

is the (one-dimensional) resolvent.

Some practical notes are given here. If the mean velocity profile, $\overline{U}(y)$, is known, then $\mathcal{H}_{\mathbf{k}}$ can be formulated for any $\mathbf{k}$. If there are no eigenvalues of $\mathcal{L}_{\mathbf{k}}$ with zero real part, then the pseudospectral interpretation of Equation 12 is clear. Note that implementing the SVD requires attention to quadrature weights to account for grid spacing and ensure that the inner product is proportional to the kinetic energy of the mode under consideration. Lastly, the SVD may be implemented in different ways. Considerable time savings can be achieved by using randomized algebra to approximate the SVD for a low-rank resolvent [4].

2 Physical interpretation of resolvent modes

Resolvent modes can be considered as describing the spatial and component-wise distributions, or mode shapes, that are most amplified by the linear dynamics of the equations of motion. The linear analysis in isolation can give no information about the relative magnitudes or phases of these modes. The forms of the resolvent modes (response and forcing pairs) impart information about the properties of the resolvent operator itself, and the physical mechanisms giving rise to amplification. The catalog of such mechanisms is large. Here a non-comprehensive list is given, with a view to categorizing origins and manifestation of a range of phenomena. More insight will be obtained by referring to analyses of specific flows in the literature.

2.1 Definitions

A *self-adjoint* operator is one that is its own adjoint, i.e. for the Hermitian case $\mathbf{A} = \mathbf{A}^*$, where $\cdot^*$ denotes the conjugate transpose. Such operators have orthogonal eigenvectors and real eigenvalues.[1]

[1]As the discussion develops, note the unfortunate difference in terminology between the exponent in the temporal Fourier transform used in resolvent analysis (purely real ω

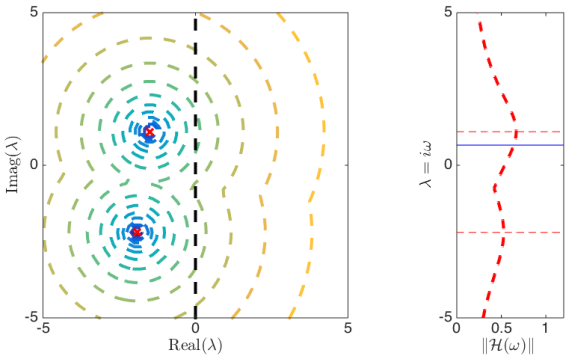

(a)

Figure 1: The eigenspectrum and pseudo-spectrum for the normal operator **S**. Eigenvalues are marked with red crosses. Color contours outline the bounds of the perturbed spectra - the ϵ-pseudospectra, for a range of constant perturbation magnitudes. The resolvent norm (right) reflects the value of these contours along the imaginary axis. Red, dashed horizontal lines indicate the resonant (eigen)frequencies of the operator. The blue, solid horizontal line represents the most highly amplified frequency in the non-normal case, i.e. operator **P**, for comparison with Figure 2. Adapted from [5].

An operator that is *normal*, but not self-adjoint, i.e. $\mathbf{A}\mathbf{A}^* = \mathbf{A}^*\mathbf{A}$, also has orthogonal eigenvectors, but the eigenvalues may be complex.

The linearized Navier-Stokes operator that is characterized in the resolvent has been known for some time to be *non-normal*, an important consequence of which is that its eigenvectors do not form an orthogonal basis.

2.2 The effect of non-normality

We will use two simple examples, as outlined in [5] in the spirit of [6], to illuminate important differences between normal and non-normal operators, which will help interpret resolvent modes.

Consider first the normal, two-dimensional operator, **S**.

$$\mathbf{S} = \begin{pmatrix} -1.5 + 1.1i & 0 \\ 0 & -1.9 - 2.2i \end{pmatrix} \tag{14}$$

gives rise to oscillatory - neutral - modes) and the usual $e^{\lambda t}$ form of perturbations in the eigenvalue problem (purely real eigenvalues, λ, correspond to exponential growth or decay.

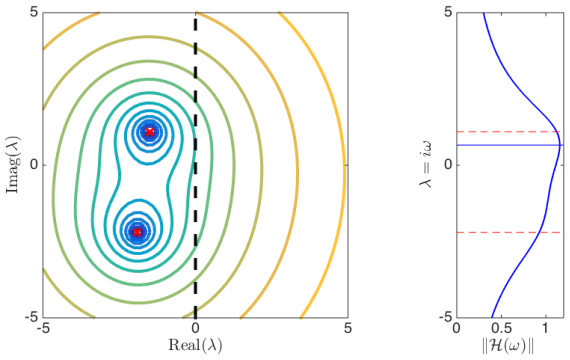

(a)

Figure 2: The eigenspectrum and pseudo-spectrum for the non-normal operator $\mathbf{P}$. Colors as in Figure 1. Adapted from [5].

The two, stable eigenvalues of $\mathbf{S}$ make up the eigenspectrum, $\mathbf{\Lambda}(\mathbf{S})$ of this operator and are identified in Figure 1. We also plot the *ϵ-pseudospectra* of $\mathbf{S}$, which correspond to level curves of the new locations of the eigenvalues of $\mathbf{S}$ when subjected to perturbations or forcing of magnitude ϵ, i.e.

$$\mathbf{\Lambda}_\epsilon(\mathbf{S}) = \{z \,\epsilon\, \mathbb{C} : z \,\epsilon\, \mathbf{\Lambda}(\mathbf{S}+\mathbf{E}) \text{ where} \|\mathbf{E}\| \leq \epsilon\} \tag{15}$$

For a normal operator, the *ϵ-pseudospectrum*, $\Lambda_\epsilon(\mathbf{S})$ is separated from $\Lambda(\mathbf{S})$ by a distance of magnitude less than or equal to ϵ. In Figure 1, this corresponds to pseudospectra which form concentric circles around the eigenvalues for small ϵ and then merge for larger perturbations. Thus we see that applying forcing to a normal operator results in a bounded movement (or sensitivity) of the eigenvalues.

For this operator, the forcing and response modes arising from the SVD of the resolvent are identical and equal to the eigenmodes, which can be checked as an exercise for the reader. In the general resolvent,

$$\psi_{j,\mathbf{S}}(\mathbf{x},\omega) = \phi_{j,\mathbf{S}}(\mathbf{x},\omega). \tag{16}$$

Since we are interested in obtaining neutrally-stable, non-growing or decaying modes from resolvent analysis, we now consider the magnitude of the pseudospectra on the real axis. This is equivalently the resolvent norm, $\|H(\omega)\|$, which can be shown to be simply the largest singular value, σ_1, and is plotted for this example on the right of Figure 1.

For a normal operator and by the logic above, the resolvent norm is inversely proportional to the distance to the nearest eigenvalue. For the operator $\mathbf{S}$, there are two peaks in $\|H(\omega)\|$, occurring at the resonant (or eigenvalue) frequencies. Note, however, that this does not imply resonant (unstable) behavior: the interpretation is that an appropriate perturbation (forcing) applied to the operator will give rise to a response in the same direction with a gain given by $\|\|H(\omega)\|$ (in this case with magnitude less than one, so still damped).

By adjusting the upper right entry in $\mathbf{S}$, the operator can be made non-normal, i.e. $\mathbf{P}$

$$\mathbf{P} = \begin{pmatrix} -1.5 + 1.1i & 5 \\ 0 & -1.9 - 2.2i \end{pmatrix} \tag{17}$$

While the eigenspectrum remains the same, i.e. $\Lambda_{\mathbf{S}} = \Lambda_{\mathbf{P}}$, the same is not true for the pseudospectra, see Figure 2. The separation between the eigenvalues of the perturbed operator and the unperturbed case can be much larger than ϵ. This implies a large sensitivity of the operator to forcing, which is reflected in the larger resolvent norm values, here exceeding one. Note also that the peak gain does not correspond to a resonant frequency in this case.

For this non-normal operator, the forcing and response resolvent modes are *not* identical,

$$\psi_{j,\mathbf{P}}(\mathbf{x}, \omega) \neq \phi_{j,\mathbf{P}}(\mathbf{x}, \omega). \tag{18}$$

Note, therefore, that resolvent analysis can differentiate between the origin of amplification due to self-adjoint, normal and non-normal mechanisms, simply by comparing forcing and response resolvent modes and eigenmodes.

Formally, the resolvent norm can be bounded [7]. If $\boldsymbol{V}$ and $\boldsymbol{\Lambda}$ are the matrix of eigenvectors and diagonal matrix of eigenvalues, respectively, then

$$\|i\omega \boldsymbol{I} - \boldsymbol{\Lambda}\|^{-1} \leq \|H(\omega)\| \leq \underbrace{\underbrace{\|\boldsymbol{V}\|\|\boldsymbol{V}^{-1}\|}_{\text{pseudo-resonance}} \underbrace{\|i\omega \boldsymbol{I} - \boldsymbol{\Lambda}\|^{-1}}_{\text{resonance}}}_{\text{resolvent}}. \tag{19}$$

Equation 19 reveals contributions from both resonant mechanisms, when the frequency corresponds to an eigenvalue, and so-called pseudoresonance associated with the non-orthogonality of the eigenvectors for a non-normal operator. See, e.g. [7] for a description of the importance of this with regards to transient growth of disturbances, [6] for more information on the implications of the various terms, and [8] and [9] for further discussion of resonant and non-resonant amplification.

2.3 The origins of amplification

Armed with the understanding of the eigen- and pseudo-spectra of normal and non-normal operators, we now consider the physical interpretation of some classes of response modes for the full NSE resolvent. Features of response modes associated with different terms and mechanisms are illustrated through (two-component) cartoons in Figure 3, which is taken from [5], with reference to properties of the NSE resolvent.

Consider first a flow without downstream development, e.g., with a one-dimensional, one component mean velocity profile. For a self-adjoint, and therefore normal, operator, forcing and response modes would be identical: Figure 3(a,b).

However the resolvent of the NSE is not normal. Even in the absence of mean shear (which makes the operator *normal*), the resolvent is not *self-adjoint* because of the imaginary terms on the operator diagonals (associated with flow advection). In this case, the forcing and response modes shapes may be similar, but with a phase shift. This manifests as a spatial shift between forcing and response in the cartoons of Figure 3(c,d). The influence of advection can be to localize both forcing and response modes around the critical layer, where the wavespeed given by $c = \omega/k_x$ is equal to the local mean velocity.

The coupling of the mean shear, $\partial\overline{U}_y$, with the wall-normal velocity gives rise to a response in different component(s) to the forcing. This *component-wise* non-normality is sketched in Figure 3(e,f). In the NSE, this effect is known as "lift-up", with the physical interpretation of v-fluctuations "lifting" fluid with low mean streamwise momentum away from the wall and bringing high streamwise momentum fluid towards the wall, an efficient method of generating energetic streamwise velocity "streaks".

The Orr mechanism corresponds to a forcing mode with upstream inclination being converted to a downstream leaning response mode, as sketched in Figure 3(g,h). This phenomenon is key in transient energy growth analysis, in which the mean profile rotates initially upstream leaning perturbations, with the peak energy extraction from the mean corresponding to when the perturbation is essentially vertical, i.e. without inclination. The interpretation in resolvent analysis does not directly correspond to temporal evolution of a particular perturbation; rather upstream leaning forcing is particularly efficient at exciting a downstream leaning response.

We shift now to mechanisms associated with spatially-developing flows.

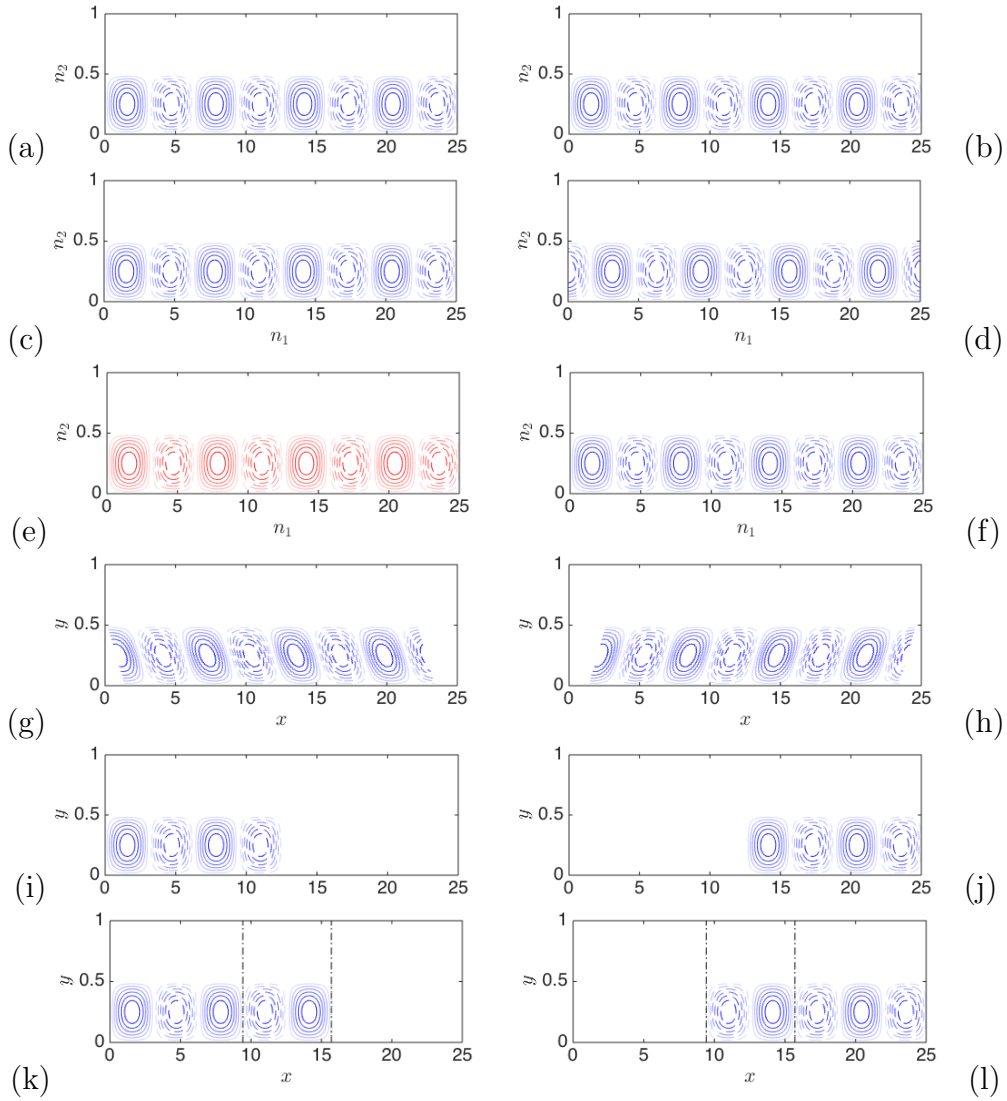

Figure 3: Cartoon showing key features of the forms of (left) forcing and (right) response modes for the following operator classifications and mechanisms. (a,b): self-adjoint, (c,d) normal but not self-adjoint and (e,f) non-normal (componentwise non-normality, "lift-up" effect) operators. (g,h): Orr mechanism. (i,j) convective-type non-normality and (k,l) overlapping forcing and response modes, indicating flow region associated with self-sustaining fluctuations. Positive contours are solid lines while negative contours are dotted lines; different colors denote different forcing/response components. Adapted from [5].

Consider, for a simple example, a two-dimensional, two-component mean field given by $\mathbf{U} = (U(x,y), V(x,y), 0)$. With direct analog to the concepts of convective and absolute instabilities in linear stability theory, two types of mechanism deriving from mean flow advection can be identified. For a *convective* non-normality, the forcing modes lie upstream and distinct from the response modes: Figure 3(i,j). Forcing and response modes may also overlap in space, Figure 3(k,l), with the region of coexistence corresponding to a location of sensitivity of the mean flow to perturbation. In stability theory, this corresponds to a region of absolute instability; for the resolvent case, the interpretation pertains to the possibility of self-sustaining fluctuations.

While the cartoons of Figure 3 sketch the simplified characteristics of the mechanisms described above, several can be active at once. Some examples will be given in the accompanying lecture.

3 Mode weights and data reconstruction

How can the basis functions obtained via resolvent analysis be exploited for qualitative insight or quantitative modeling? We have discussed some of the information that can be gleaned about the mode shapes and relationships between forcing and response associated with different physical mechanisms in the previous section. In this section, we tackle the problem of determining how strongly each mode appears in a real flow once the resolvent basis functions have been obtained. The mode weights may be determined by the distribution of nonlinear interactions in turbulent flows, such that the full system of Equation 12 is self-consistent, or by, for example, an external perturbation in transitional flow.

If a complete representation of the full field is available, *data-driven* basis functions that are analogous to the *equation-driven* resolvent basis may be obtained by such techniques as proper orthogonal decomposition (POD), spectral POD and dynamic mode decomposition. Crudely put, these techniques all obtain basis functions ranked by energy in the real flow. Thus the question of determining the weights on the resolvent modes is intimately related to the connection between the data- and equation- driven approaches. Useful discussions of these connections are summarized in [8] and [10].

Returning to Equation 8, we see that knowledge of the mean field alone provides both the basis functions, $\psi_j(\mathbf{x},\omega)$ and $\phi_j(\mathbf{x},\omega)$ and the singular values, $\sigma_j(\omega)$. Thus only the weights, $\chi_j(\omega)$, remain to be determined. These

are complex, i.e. they have both magnitude and phase.

We move beyond the linear basis that can be obtained from the SVD to consider the mode weights that correspond to the real flow, how these can be used to reconstruct the state vector where it was not measured, and associated nonlinear interactions and their relationship to the sustaining mechanisms of turbulence.

3.1 Modeling mode weights

The simplest model for the weights is broadband forcing: every singular forcing mode is excited with unit amplitude, for every frequency. The output is then dictated solely by the resolvent, since the output is given by Equation 8, with $\chi_j(\omega) = 1$ for all ω. If the resolvent is low rank, it can be approximated with just a few singular modes at each frequency. Such an approach does not give rise to any information on the relative phases between the $\chi_j(\omega)$'s, thus its usefulness is usually limited to crude modeling of the variance of the fluctuation energy.

The use of an eddy viscosity, $\nu_T(\mathbf{x})$, in the resolvent formulation itself can be considered as one way of providing a more sophisticated variation of forcing amplitude. This typically corresponds to variation as a function of spatial coordinates through the assumed eddy viscosity profile, rather than by frequency or scale.

Along a similar vein to broadband forcing, stochastic (white noise) forcing of the input to the full system can be employed [3]. This input can be shaped or "colored" to optimally reproduce flow statistics obtained from data [11], an approach which is directly connected to the subject of the next section.

3.2 Determining mode weights from data

Mode weights may be obtained directly from data, for example by approximating the real field by a truncated sum of N modes per frequency

$$\mathbf{u}(\mathbf{x}, t) \approx \sum_{j=1}^{N} \chi_j(\omega)\psi_j(\mathbf{x}, \omega)e^{i\omega t}, \tag{20}$$

and solving a least squares problem for $\chi_j(\omega)$ based on data at a restricted number of spatial (sensor) locations, $\mathbf{x_0}$, i.e. minimizing

$$\varepsilon = \mathbf{u}(\mathbf{x_0}, t) - \sum_{j=1}^{N} \chi_j(\omega)\psi_j(\mathbf{x_0}, \omega)e^{i\omega t} \tag{21}$$

subject to some norm. Techniques exist to solve this problem in the Fourier domain; care must be taken to preserve phase information when Fourier transforming the data.

Clearly the choice of sensor locations, $\mathbf{x_0}$, is important. If a mode has no physical footprint at $\mathbf{x_0}$, then $\chi_j(\omega) = 0$ will be determined and the mode cannot be captured.

Alternatively, an optimization procedure may be performed to determine the assembly of modes which best reproduces a given aspect of the dataset.

Some examples of approximating mode weights from data will be given in the accompanying lecture.

3.3 Modeling and data reconstruction

Low-order models may be constructed based on the correctly weighted resolvent modes. Especially for flows close to transition or oscillator-type flows, such models can be very effective. Early work by Gomez *et al.* [12] and Beneddine *et al.* [13] applied these techniques to lid-driven cavity and a backward facing step, respectively.

Alternatively, if spatially- and temporally-resolved information is not available in some part of the flow domain, but the mean field is, then the weighted resolvent basis may be used to approximate the missing data. Once complex mode weights are known, per the preceding section, it is a simple matter to evaluate the modes in the region of missing data and to evolve the model in time.

3.4 Nonlinear interactions

Information pertaining to mode weights may also be garnered by explicitly considering the nonlinear interactions between resolvent modes that are triadically related via $\mathbf{k}'' = \mathbf{k} - \mathbf{k}'$, via a nonlinear interaction coefficient [14],

$$\mathcal{N}_{lij}(\mathbf{k}, \mathbf{k}') = -\sigma_i(\mathbf{k}')\sigma_j(\mathbf{k}'')\langle\phi_l^*(y, \mathbf{k}) \cdot (\psi_i(y, \mathbf{k}') \cdot \nabla\psi_j(y, \mathbf{k}''))\rangle. \tag{22}$$

This approach remains relatively underdeveloped at this time, due mostly to the wider range of scales (and therefore number of potential nonlinear interactions) involved in most flows of interest, although some selection rules do exist.

4 Incorporating control

In order to incorporate control, we return to the state space representation of Equation 1, in which ζ describes and external control input. Linear control laws pertaining to the fluctuations may also be directly implemented in the resolvent. A brief description of both approaches, as well as the fundamental guidance concerning the sensitivity of a flow obtained via the uncontrolled resolvent, is given in this section.

4.1 Sensitivity to forcing

At the simplest level, the uncontrolled resolvent analysis described above provides important insight into forcing inputs which are highly amplified, their frequencies and spatial footprint. For a researcher looking to simply manipulate a flow, this is first order information: aligning external actuation as closely as possible to the first forcing modes should result in a change to the flow state through linear amplification and subsequently modified nonlinear interactions. The sense of this change relative to a global objective is not determined, however.

Yeh & Taira [15] employed this kind of approach to guide the choice of frequency and spanwise wavelength for actuators on the surface of an airfoil in order to control flow separation. They concluded that their resolvent approach, which used the uncontrolled mean field from large eddy simulation, correctly identified both the range of actuation frequencies for which separation was impacted and global changes to the flow field.

The sensitivity can be defined with regards to any output of interest by appropriate adjustment of $\mathcal{C}$ in Equation 2. For example, [16] use a formulation which permits isolation of jet noise in this kind of analysis.

4.2 Control through boundary conditions

Linear control techniques acting on the fluctuations can be incorporated into resolvent analysis. For example, a fluctuating boundary velocity that is not the usual no-slip, no-penetration boundary condition, but rather is related to the velocity within the domain, may be imposed on a mode-by-mode basis. For example, consider constraining the v-velocity at the wall in turbulent channel flow to have the same magnitude but opposite sign to the v signal at a detector plane at a fixed height, y_d, above the wall. This control technique is known as opposition control [17], and has been studied in detail (at relatively low turbulent Reynolds numbers) through direct numerical simulation.

In terms of the resolvent, this boundary condition can be implemented directly as

$$\hat{v}(\mathbf{k}, y_w) = -A_d \hat{v}(\mathbf{k}, y_d), \tag{23}$$

with A_d=1, where y_w is the wall-normal location of the wall.

The result of applying this boundary condition for a given resolvent mode depends on whether or not the uncontrolled mode has a v signature at y_d. If it does, then opposition control leads to a controlled mode shape with zero v somewhere between y_w and y_d, which is consistent with the idea proposed in the original studies of a "virtual wall", which acts to prevent high-speed fluid being swept down to the wall in analogy to the lift-up effect. Thus empirical insight is reflected in resolvent modes derived from the NSE. Further, the amplification for such controlled modes, i.e. the singular values, can also be modified due to the opposition control boundary condition, suggesting a broader change to the nonlinear interactions sustaining the controlled flow (and therefore also the mean velocity - see below).

Resolvent analysis allows the investigation of variations on Equation 23, for example the influence of the location of the detector plane, y_d, or adding a complex component to A_d, which is equivalent to adding a spatio-temporal phase shift between the detector and wall signals. Percolating the net change in Reynolds stresses due to the opposition control boundary condition under broadband forcing through to the net drag for various values of y_d the parameter ranges for net drag reduction and increase appear to be well captured by [18]

Expanding the range of conditions that had been explored in DNS, Luhar *et al.* [18] also used the resolvent approach to propose that the maximum drag reduction would occur for $A_d = e^{i\alpha}$, where α represents a (temporal or spatial) phase shift between the signals at the detection plane and the wall,

an hypothesis which has subsequently been borne out by the comparison between direct numerical simulation and resolvent approximations [19].

4.3 External control

Application of resolvent analysis to the design of full closed loop controllers, as expressed in Equation 1, requires knowledge of the controlled mean field, which may not be easily obtained. The steps described above can be employed in the absence of the controlled mean, i.e. simply using the uncontrolled mean field and accepting a modeling error, or an iterative procedure can be implemented[20]. In the latter approach, resolvent analysis is first used to design a controller for specific features of the uncontrolled mean. Control drives the flow to a new dynamical equilibrium, with a new mean. Subsequent controllers are then designed for further suppression of fluctuations.

Exploiting resolvent analysis to investigate control techniques is an active area of research.

5 Close

There exists a range of literature covering foundational aspects of resolvent analysis and applied to several different flows. It is hoped that these notes and accompanying lecture provide an introduction to the topic that expedites a more complete understanding of ongoing research in the area.

References

[1] A. S. Sharma. Elements of resolvent methods in fluid mechanics: notes for an introductory short course. EPSRC Summer School on Modal Decompositions in Fluid Mechanics, 2019.

[2] M. R. Jovanović and B. Bamieh. Componentwise energy amplification in channel flows. *J. Fluid Mech.*, 534:145–183, 2005.

[3] Y. Hwang and C. Cossu. Linear non-normal energy amplification of harmonic and stochastic forcing in the turbulent channel flow. *J. Fluid Mech.*, 664:51–73, 2010.

[4] N. Halko, P. G. Martinsson, and J. A. Tropp. Finding structure with randomness: Probabilistic algorithms for constructing approximate matrix decompositions. *SIAM Review*, 53(2):217–288, 2011.

[5] S. Symon, K. Rosenberg, S. T. M. Dawson, and B. J. McKeon. Non-normality and classification of amplification mechanisms in stability and resolvent analysis. *Phys. Rev. Fluids*, 3(053902), 2018.

[6] T. Gebhardt and S. Grossmann. Chaos transition despite linear stability. *Phys. Rev. E*, 50(5):3705, 1994.

[7] P J Schmid and D S Henningson. *Stability and Transition in Shear Flows*. Springer-Verlag, New York, 2001.

[8] K. Taira, S. L. Brunton, S. T. M. Dawson, C. W. Rowley, T. Colonius, B. J. McKeon, O. T. Schmidt, S. Gordeyev, V. Theofilis, and L. S. Ukeiley. Modal analysis of fluid flows: An overview. *AIAA J.*, 55 (12):4013–4041, 2017.

[9] P. J. Schmid. Nonmodal stability theory. *Annu. Rev. Fluid Mech.*, 39:129–162, 2007.

[10] A. Towne, O. T. Schmidt, and T. Colonius. Spectral proper orthogonal decomposition and its relationship to dynamic mode decomposition and resolvent analysis. *J. Fluid Mech.*, 847:821–867, 2018.

[11] A. Zare, M. R. Jovanović, and T. T. Georgiou. Color of turbulence. *J. Fluid Mech.*, 812:636–680, 2017.

[12] F. Gómez Carrasco, H. Blackburn, M. Rudman, A. Sharma, and B. McKeon. A reduced-order model of three-dimensional unsteady flow in a cavity based on the resolvent operator. *J. Fluid Mech.*, 798:R2, 2016.

[13] S. Beneddine, D. Sipp, A. Arnault, J. Dandois, and L. Lesshafft. Conditions for validity of mean flow stability analysis and application to the determination of coherent structures in a turbulent backward facing step flow. *J. Fluid Mech.*, 798:485–504, 2016.

[14] B. J. McKeon, A. S. Sharma, and I. Jacobi. Experimental manipulation of wall turbulence: a systems approach. *Phys. Fluids*, 25(031301), 2013.

[15] C.-A. Yeh and K. Taira. Resolvent-analysis-based design of airfoil separation control. *J. Fluid Mech.*, 867:572–610, 2018.

[16] J. Jeun, J. W. Nichols, and M. R. Jovanović. Input-output analysis of high-speed axisymmetric isothermal jet noise. *Phys. Fluids*, 28(4):047101, 2016.

[17] H Choi, P Moin, and J Kim. Active turbulence control for drag reduction in wall-bounded flows. *J. Fluid Mech.*, 262, 1994.

[18] M. Luhar, A. S. Sharma, and B. J. McKeon. Opposition control within the resolvent analysis framework. *J. Fluid Mech.*, 749:597–626, 2014.

[19] S. S. Todtli, M. Luhar, and B. J. McKeon. Predicting the response of turbulent channel flow to varying-phase opposition control: resolvent analysis as a tool for flow control design. *Phys. Rev. Fluids*, (to appear).

[20] C. Leclercq, F. Demourant, C. Poussot-Vassal, and D. Sipp. Linear iterative method for closed-loop control of quasiperiodic flows. *J. Fluid Mech.*, 868:26–65, 2019.